ACS APPLIED ELECTRONIC MATERIALS

pubs.acs.org/acsaelm Article

Dominant Effects of Epitaxial Strain on the Phase Control of Heterostructural $(In_xGa_{1-x})_2O_3$ Alloys

Han Uk Lee,[‖] Hyeon Woo Kim,[‖] Giulio Fatti, Hyunseok Ko, and Sung Beom Cho*

Cite This: *ACS Appl. Electron. Mater.* 2022, 4, 2711−2717 Read Online

ACCESS | Metrics & More | Article Recommendations | Supporting Information

ABSTRACT: While $(In_xGa_{1-x})_2O_3$ alloy is a crucial system for the Ga_2O_3-based ultrawide bandgap semiconductor application, its successful phase control has been struggling because of its heterostructural nature and rich polymorphs. Here, we identified the thermodynamic phase diagrams for both the bulk state and epitaxial state of $(In_xGa_{1-x})_2O_3$ alloy by using comprehensive density afunctional theory (DFT) calculations and regular solution models, which is consistent with previous experimental reports. By comparing the phase diagrams under a strain-free condition and an epitaxial strain condition, we demonstrate that the epitaxial strain is a significant factor in the successful growth of alloys in heteroepitaxy processes. While the alloying of $(In_xGa_{1-x})_2O_3$ is limited by a miscibility gap under the strain-free condition, the Al_2O_3 heteroepitaxy substrate opens more metastable regions for various polymorphs. With the choice of a suitable substrate, we also suggest the phase control strategy for $(In_xGa_{1-x})_2O_3$ alloys in orthorhombic polymorphs.

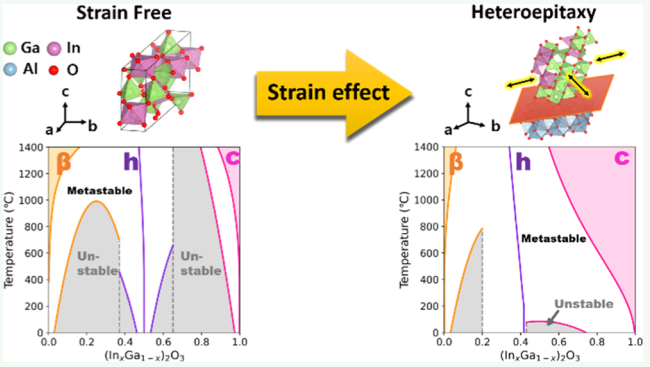

KEYWORDS: *gallium oxides, density functional theory, heteroepitaxy, phase diagram, epitaxy engineering*

INTRODUCTION

Ga_2O_3 is rapidly emerging as a promising material for the next generation of high-power electronics and optoelectronics due to its attractive properties such as an ultrawide bandgap and a high breakdown field.[1,2] The fascinating feature of Ga_2O_3 is the possibility of engineering the bandgap by alloying it with different elements such as Al[3−5] or In,[6,7] thus controlling the diversiform polymorphs.[8,9] By incorporating Al or In into Ga_2O_3 to form ternary alloys, that is, $(Al_xGa_{1-x})_2O_3$,[5,10−12] and $(In_xGa_{1-x})_2O_3$,[13−15] the bandgap can be adjusted over a wide range from 2.9 to 8.8 eV.[13,16] These heterostructural solid solutions, because their end members have different ground state structures, also provide the possibility of controlling the crystal structure by adjusting the concentration of Al or In compositions. For $(Al_xGa_{1-x})_2O_3$, the thermodynamic behavior has been theoretically elucidated,[16,17] and it has been successfully fabricated through novel methods.[18] On the other hand, the phases of $(In_xGa_{1-x})_2O_3$ alloy are relatively more difficult to control because of the large difference of atomic radius between Ga and In atoms, which causes the existence of an intermediate metastable phase.[19] Therefore, a deeper understanding of the phase stability is necessary to successfully synthesize the $(In_xGa_{1-x})_2O_3$ alloy systems.

Despite the numerous attempts to grow $(In_xGa_{1-x})_2O_3$ alloy systems using epitaxy to obtain high-quality single-phase thin films, they have been inconsistent to date.[20−23] Recently, for successful growth, the bulk phase diagram of this alloy has been suggested.[24] However, the proposed results remain controversial as there are reports of epitaxial thin-film growth inconsistent with these findings.[21,25,26] The discrepancies are due to a lack of an understanding of the relation between phase competition and the strain occurring in the epitaxial process. In the heteroepitaxy process, the strain affecting the quality of the layer is mainly due to (1) the lattice mismatch between the substrate and the growing thin film and (2) the lattice stretching of $(In_xGa_{1-x})_2O_3$ caused by the increasing molar concentration of In. Therefore, the effect of both the substrate and In molar concentration should be carefully investigated for the successful growth of the $(In_xGa_{1-x})_2O_3$ alloy.

In this work, we investigated the stability of the heterostructural $(In_xGa_{1-x})_2O_3$ alloy system as a function of the molar concentration using first-principles calculations combined with the regular solution model. We calculated the phase diagrams for both the bulk-state and the epitaxial-state, that is, under strain conditions, to schematize their phase stability upon alloying. We found that the epitaxial growth dramatically changes the favorable phases, depending on the

Received: February 18, 2022
Accepted: May 12, 2022
Published: May 24, 2022

https://doi.org/10.1021/acsaelm.2c00240
ACS Appl. Electron. Mater. 2022, 4, 2711−2717

choice of the substrate. We proved, therefore, that a careful choice of the substrate is a necessary phase control strategy. Based on this analysis, we recommended $LiTaO_3$, a commercially available substrate, to grow ε-$(In_xGa_{1-x})_2O_3$ alloys.

COMPUTATIONAL METHOD

Density functional theory (DFT) calculations were performed using Vienna Ab-initio Simulation (VASP) package[27] and the projector-augmented wave method.[28] The electronic wave functions were expanded in plane waves with a cutoff energy of 520 eV to minimize Pulay stress during the structural optimization. The structural optimization was truncated when the Hellmann−Feynman forces reached the threshold value of 0.001 eV/Å. The Brillouin zone was sampled using a 100 k-points density per 1 Å^3 in the reciprocal cell. The 3d, 4s, and 4p states of Ga, 5s, 4d and 5p states of In, and 2s and 2p states of O were taken into account as valence states, and the exchange−correlation energy of valence electrons was described by the Perdew−Burke−Ernzerhof (PBE)[29] parametrization of the generalized gradient approximation (GGA). As PBE is known to overestimate the lattice constants, to keep the consistency, we have used PBE-optimized lattice constants for all Ga_2O_3 polymorphs and substrates, as shown in Supporting Information Table S1. We modeled $(In_xGa_{1-x})_2O_3$ random alloy systems by special quasirandom structures (SQS)[30] using the *mcsqs* code provided in the alloy theoretic automated toolkit (ATAT).[31] We selected the number of atoms in the range of 80 to 480 for all SQS cells to obtain the fully converged energy of alloy systems. To evaluate the epitaxial strain, we generated the slabs by considering the epitaxial relation between the substrates and $(In_xGa_{1-x})_2O_3$ alloy by CSL theory[32] (see the Supporting Information Figure S3) and fixed a, b axes with the same lattice constant of the substrate.

RESULTS AND DISCUSSION

In order to study the heterostructural $(In_xGa_{1-x})_2O_3$ alloy systems, it is essential to understand the structural features of the solid solution in the alloying process as a function of the molar concentration and temperature. This problem is not trivial because the ground states of the solid solution endmembers have very different crystal structures, Ga_2O_3 being monoclinic in the β-phase and In_2O_3 a cubic bixbyite in its c-phase. Additionally, Ga_2O_3 has various polymorphs,[8,9] namely α-(corundum), ε-phases (orthorhombic), and also h-$InGaO_3$ (hexagonal) alloy has been observed experimentally.[19] Furthermore, these polymorphs consist of three types of polyhedral sites, such as tetra-, penta-, and octahedral sites. In Figure 1, the aforementioned atomic structures and polyhedral sites are depicted. Interestingly, in the alloying process of the $(In_xGa_{1-x})_2O_3$ systems, In atoms have been experimentally identified to occupy only the octahedral site because it optimizes the bonding length with anions.[13,19,33,34] This behavior is well-explained by considering the correlation of the coordinated number for the In atom and the average In−O bonding length in the work by Farvid *et al.*[35] This indicates that indium being incorporated on the tetra- or pentahedral sites is energetically unfavorable. Therefore, to compute the total energy of the $(In_xGa_{1-x})_2O_3$ alloy systems, the stability of each alloy phase needs to be carefully calculated.

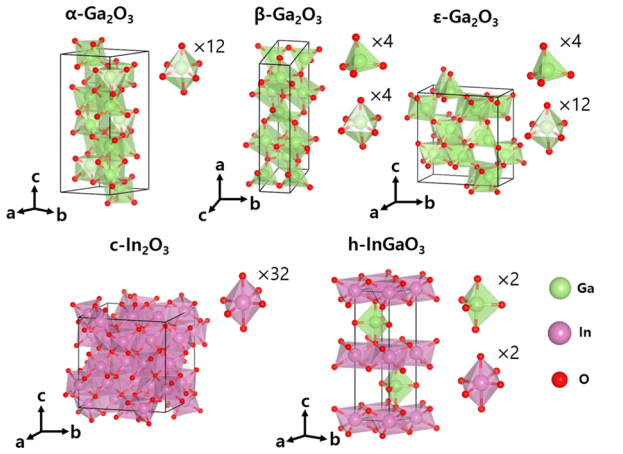

Figure 1. Atomic structures of Ga_2O_3 polymorphs for α(corundum), β(monoclinic), and ε(orthorhombic), c-In_2O_3 for cubic bixbyite, and h-$InGaO_3$ for hexagonal. The light green, pink, and red atoms represent Ga, In, and O, respectively.

To model the alloying process considering the site preference, we prepared three types of alloy models, the fully disordered, the quasidisordered, and the fully ordered, each with different In concentrations. We generated the fully disordered structure to mimic the alloying process of α- and c-phases. The α- and c-phases, indeed, consist only of octahedral sites; thus, Ga and In atoms could be randomly incorporated in these cation sites covering the full range of the In concentration. The other phases are composed of mixed polyhedral sites; thus, the In atoms occupy, first, the octahedral sites of the unit cells, and only later, as the In concentration increases, they are substituted by Ga atoms at tetra- or pentahedral sites. To model this alloying behavior, we have designed the quasidisordered structure. Finally, to consider all the In and Ga atoms positioned only at their preference sites in the alloy, we constructed the fully ordered structure. The structures of the fully-, quasidisordered, and fully ordered are represented in Figure 2a. For the detailed structure of the $(In_xGa_{1-x})_2O_3$ polymorphs, see Supporting Information Figure S1.

We then investigated the phase stability of the different structures. The phase stability is determined by the Gibbs free energy of mixing, given by the relation

$$\Delta G_{mix}(x,\ T) = \Delta H_{mix}(x) - T\Delta S_{mix}(x) \quad (1)$$

where T is the temperature, $\Delta H_{mix}(x)$ is the enthalpy, and $\Delta S_{mix}(x)$ is the entropy of mixing. The enthalpy of mixing identifies the correlation between the site preference and the stability as a function of the molar concentration and is defined as

$$\Delta H_{mix}[(In_xGa_{1-x})_2O_3] = E[(In_xGa_{1-x})_2O_3] - (1-x)E[Ga_2O_3] - xE[In_2O_3] \quad (2)$$

where $E[(In_xGa_{1-x})_2O_3]$ is the total energy of the SQS supercell structure of the random alloy and $E[Ga_2O_3]$ and $E[In_2O_3]$ are the total energies of ground states of Ga_2O_3 and In_2O_3. This can be expressed with the regular solution model for the heterostructural alloy[16] in the form of

$$\Delta H_{mix}(x) = (1-x)\Delta H_{Ga_2O_3} - x\Delta H_{In_2O_3} - x(1-x)\Omega \quad (3)$$

https://doi.org/10.1021/acsaelm.2c00240
ACS Appl. Electron. Mater. 2022, 4, 2711−2717

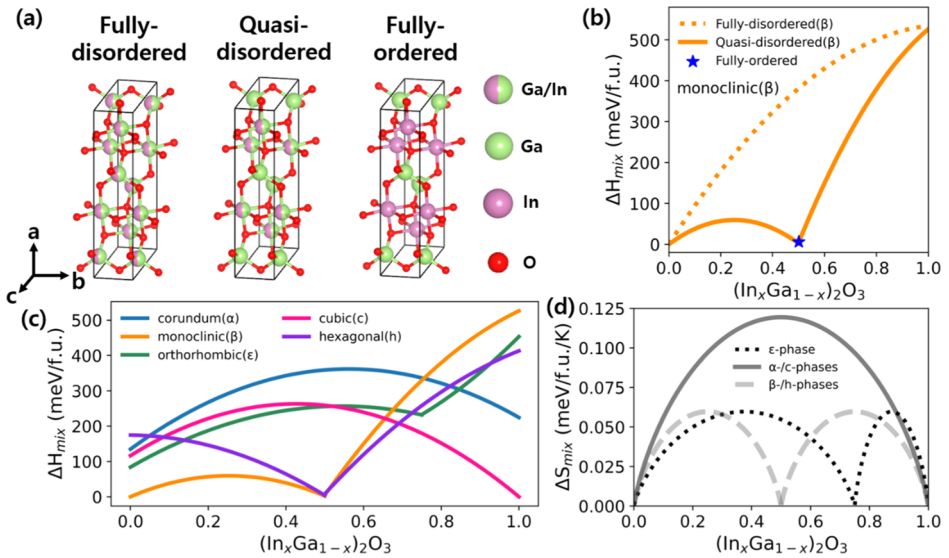

Figure 2. (a) Atomic structures of $(In_xGa_{1-x})_2O_3$ for the fully disordered, quasidisordered, and fully ordered lattice. The half-pink and half-light green atoms represent random occupations of Ga and In atoms. The light green, pink, and red atoms represent Ga, In, and O, respectively. (b) Comparison between the enthalpies of mixing of the fully disordered, quasidisordered, and fully ordered $(In_xGa_{1-x})_2O_3$ alloy in the β(monoclinic)-phase as a function of the molar concentration. The dotted and solid orange lines represent the fully disordered and quasidisordered structures, respectively, while the blue star point represents the fully ordered structure. (c) Enthalpies of mixing of $(In_xGa_{1-x})_2O_3$ alloy systems. The light blue, orange, green, pink, and purple lines represent corundum, monoclinic, orthorhombic, cubic, and hexagonal $(In_xGa_{1-x})_2O_3$ alloy systems, respectively. (d) Entropies of mixing for the $(In_xGa_{1-x})_2O_3$ alloy systems. The dotted, solid, and dashed lines represent the entropies of mixing for the ε-phase, α-/c-phases, and β-/h-phases, respectively.

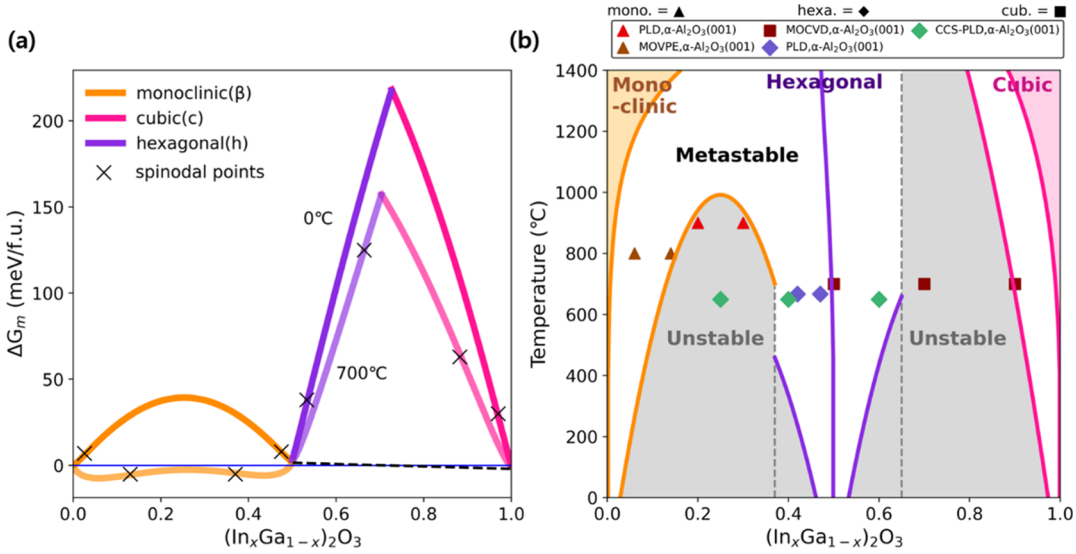

Figure 3. (a) Gibbs free energy of mixing of $(In_xGa_{1-x})_2O_3$ alloy systems at 0 and 700 °C. The orange, purple, and pink line represent, respectively, the monoclinic, hexagonal, and cubic phases. The spinodal points are indicated with black crosses. The blue solid line represents the zero value of the Gibbs free energy of mixing. The common tangent line at 700 °C in the range between 0.5 and 1.0 of the molar concentration is represented by the dashed black line. (b) Calculated bulk phase diagram of $(In_xGa_{1-x})_2O_3$ alloy systems with marked experimental values. The shaded region with orange, purple, and pink represents stable states of alloy in monoclinic, hexagonal, and cubic, respectively. The metastable regions are depicted in white, and the expected unstable regions are in grey. Triangle, diamond, and square markers represent the experimentally reported structures of monoclinic, hexagonal, and cubic, respectively.

where x is the molar concentration, $\Delta H_{Ga_2O_3}$ and $\Delta H_{In_2O_3}$ are the enthalpies of the endpoints for Ga_2O_3 and In_2O_3, and Ω is the bonding interaction parameter between the atomic species. We sampled five different points of x = 0, 0.25, 0.5, 0.75, 1 and evaluated the Ω parameter by fitting the single-parabolic equation. Based on the extracted Ω values, we found the enthalpies of mixing for all $(In_xGa_{1-x})_2O_3$ polymorphs.

Regarding β-, ε-, and h-structure, we found that the quasidisordered and the fully ordered enthalpies of mixing are much stabler than the fully disordered. The enthalpies of mixing for the β-phase are shown in Figure 2b as an example (enthalpies of mixing for ε-/h-phases represented in the Supporting Information Figure S2). The system which has a lower energy is stable in terms of thermodynamics, that is, the In prefers to cooperate with the octahedral site, first, from 0 to

https://doi.org/10.1021/acsaelm.2c00240
ACS Appl. Electron. Mater. 2022, 4, 2711−2717

Table 1. Relationship Between Strain and Changes in the Enthalpy of Mixing for Each Ground State of an Alloy Phase Grown on Various Substrates[a]

		substrate					
		α-Al_2O_3 (001)			$LiTaO_3$ (001)		
		strain (%)		$H_{epitaxy} - H_{bulk}$ (meV/f.u.)	strain (%)		$H_{epitaxy} - H_{bulk}$ (meV/f.u.)
structure	material	a	b		a	b	
corundum (α)	α-Ga_2O_3	−5.17	−5.17	404.670	2.43	2.43	76.245
monoclinic (β)	β-Ga_2O_3	−1.92	−0.22	117.099	6.12	−3.78	262.305
orthorhombic (ε)	ε-Ga_2O_3	−6.28	−5.49	401.035	1.23	2.08	27.228
cubic (c)	In_2O_3	−1.00	−1.00	9.028	6.94	6.94	364.159
hexagonal (h)	$InGaO_3$	−4.95	−4.95	316.256	2.67	2.67	65.095

[a]The chosen substrates are α-Al_2O_3 (001) and $LiTaO_3$ (001).

50% concentration (for the ε-phase, it is 75% since its cation ratios are 3:1, see Figure 1) compared to the In occupied with the tetrahedral site. For higher concentrations of In, instead, the enthalpy of mixing sharply increases because the In atoms must necessarily fit in tetra- or pentahedral sites. Contrariwise, the enthalpy of mixing of the α- and the c-phase of the alloy shows a parabolic shape over the whole In compositions range, as the structures are made only of octahedral sites. The enthalpies of mixing of all alloy phases are represented in Figure 2c.

Other than the composition, temperature also plays an important role in determining phase stability. The Gibbs free energy depends on the temperature through the term ΔS_{mix}, as shown in Figure 2d. ΔS_{mix} is the entropy of mixing, related to the concentration of Ga and In ions in the mixing process and is defined as

$$\Delta S_{mix}(x) = -Nk_B[x\ln(x) + (1-x)\ln(1-x)] \quad (4)$$

where k_B is the Boltzmann constant value of 8.617×10^{-5} (eV/K), N is the cation site degeneracy. N is defined differently for fully and quasidisordered and fully ordered structures, as explained in the work by Wouters *et al.*[24] In α-/c-$(In_xGa_{1-x})_2O_3$, which is a fully disordered structure, N is 2 as all cations are randomly occupied with the octahedral sites. In the quasidisordered β-/ε- and h-alloys, instead, N is 1 because Ga ions occupy only tetra- and pentahedral sites, while In atoms randomly occupy all cation sites in the unit cell as the concentration increases. In the fully ordered structure of these phases, N is zero as all cations are fixed in their preference cation sites. Note that the N is zero at 0.5 for β-/h-phases, which have a 1:1 cation site ratio, while N is zero at 0.75 for the ε-phase having a 3:1 cation site ratio, as shown in Figure 1. The vibrational entropy is negligible compared to the configuration entropy because its range is between the 10^{-7} and 10^{-9} eV/cation as a function of T and x.[24]

We calculated this contribution at 700 °C, where the alloying process is reported to take place on average[25,36,37] and at 0 °C. We found that the monoclinic, hexagonal, and cubic phases participated in the phase competition among the five phases, as shown in Figure 3a. To schematize the stability of the alloying process, it is necessary to calculate the phase diagram, which is determined by spinodal and binodal lines. The spinodal line is defined by the condition that the second derivative of the Gibbs free energy with respect to x is zero, $d^2/dx^2(\Delta G_{mix}) = 0$, which delimits the miscibility gap. In the region where $d^2/dx^2(\Delta G_{mix}) < 0$, the alloy is unstable with respect to minor fluctuations in the molar concentration, which leads to a phase separation known as spinodal decomposition. The binodal line is defined as the common tangent to the Gibbs free energy of mixing. Between the spinodal and binodal lines, where $d^2/dx^2(\Delta G_{mix}) > 0$, once an alloy structure is formed in a single phase, spontaneous decomposition does not occur although it is not in thermal equilibrium, and the resulting structure is metastable. Above binodal lines, the alloy structure is in its thermodynamically stable homogeneous phase.

In the calculated phase diagram of the bulk state $(In_xGa_{1-x})_2O_3$ as shown in Figure 3b, it can be seen that the unstable region is wider, whereas both stable and metastable regions occupy narrow regions of the diagram. Even though a significantly wide unstable region is observed, there are successful experimental reports that show growth by pulsed-laser deposition (PLD),[25,36,38] metal−organic vapor phase epitaxy (MOVPE),[26] and metal−organic chemical vapor deposition (MOCVD),[37] which are presented as symbols in Figure 3b. Even for the powder sintering approach in ref 34, although the two distinguished regions are observed as well, the unstable region is not thoroughly analyzed and lacks microscopic observation, and numerous reports identified that these regions are subdivided. The same issue has been reported in ref 24, consistently with our calculations. However, the successful synthesis of the monoclinic, hexagonal, and cubic structures has been reported also in the unstable region.[25,26,37] This inconsistency can be explained by considering that the strain induced by the heteroepitaxial growth affects the stability conditions of the alloy. Indeed, in the $(In_xGa_{1-x})_2O_3$ heteroepitaxial growth, the lattice parameter for each phase is fixed by the lattice parameter of the substrate, regardless of the alloy lattice parameter. This inevitably causes strain which affects the thermodynamic stability of the alloy. However, this also means that, in principle, it is possible to control the energetical stability by a suitable choice of substrate.[39] Therefore, it is important to quantify how much the strain affects the phase stability to clearly understand the heteroepitaxial growth of the solid solution.

We then focused on identifying the parameters influencing the epitaxial strain and examined whether it is indeed possible to obtain the desired phase by selecting the substrate. We looked into the lattice mismatch occurring between the substrate and the alloy thin film, which is the most important parameter affecting the strain. Moreover, since the lattice parameter stretching, according to Vegard's law,[40,41] may enhance the strain with an increasing In concentration, both factors must be taken into account to investigate the thermodynamic stability of each phase under epitaxial strain. The epitaxial enthalpies of mixing over theα-Al_2O_3(001)

https://doi.org/10.1021/acsaelm.2c00240
ACS Appl. Electron. Mater. 2022, 4, 2711−2717

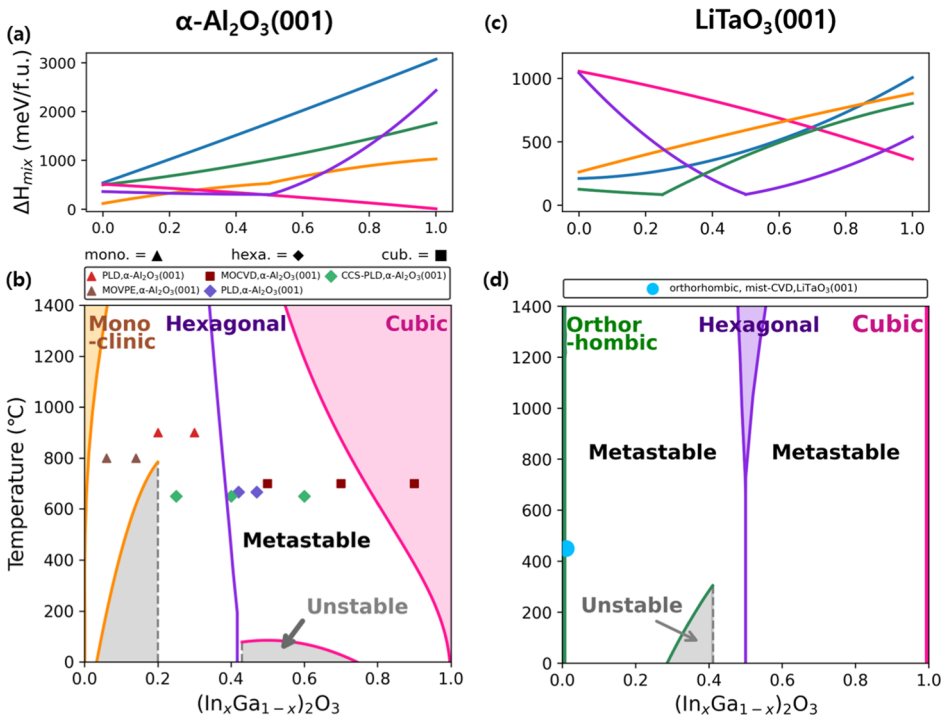

Figure 4. (a,c) $(In_xGa_{1-x})_2O_3$ enthalpies of mixing under epitaxial strain over (a) α-Al_2O_3(001) and (c) $LiTaO_3$(001) substrates. (b,d) Epitaxial phase diagram of $(In_xGa_{1-x})_2O_3$ grown on (b) α-Al_2O_3(001) and (d) $LiTaO_3$(001) substrates. The orange, green, pink, and purple regions represent the stable states of the alloy in monoclinic, orthorhombic, cubic, and hexagonal structures, respectively. White and grey regions represent the metastable and unstable states of the alloy. Triangle, diamond, square, and circle markers are the experimental reports of monoclinic, hexagonal, cubic, and orthorhombic phases.

substrate are compared with the bulk enthalpies of the end members of the alloy in Table 1. We chose α-Al_2O_3(001) as it is one of the most common substrates for the $(In_xGa_{1-x})_2O_3$ epitaxial growth.

To identify the correlation between strain and stability, we calculated the epitaxial enthalpy of mixing for each alloy phase and compared them with the bulk enthalpies. By looking at the enthalpies of mixing under the epitaxial strain shown in Figure 4a, it can be observed that the three phases (β-, h-, and c-phase) participate in phase competition the same as bulk-$(In_xGa_{1-x})_2O_3$ system. We also identified the same result in the Gibbs free energy of mixing and represented it in Supporting Information Figure S3a. However, the corresponding phase diagram, as shown in Figure 4b, represents a significant difference from the bulk phase diagram. The wider stable, metastable, and narrower unstable regions could be observed compared with the bulk diagram, which were elucidated by a more clarified experimental report of the growth on the unstable regions, which could not be explained by the bulk diagram. Specifically, the experimentally observed monoclinic phase (*i.e.*, x = 0.2 and 0.3, annealed 900 °C),[38] the hexagonal phase (*i.e.*, x = 0.22, 650 °C),[25] and the cubic phases (*i.e.*, x = 0.7, 700 °C, and x = 0.9, 700 °C)[37] lied in the "unstable" region of the bulk phase diagram, as shown in Figure 3b. This result signified that strain is a crucial parameter affecting thermodynamic behavior in addition to the molar concentration and temperature in heteroepitaxy.

Even if the strain effect plays a significant role in phase competition, the atomic configuration changes due to the interfaces, surfaces, and defects can affect the phase competition during epitaxy processes. These effects have the potential to cause the nucleation of a new metastable phase, and they should compete with the strain effect. The nucleation effect becomes more prominent when the deposition layer is thin, and the metastable phase is often observed. On the other hand, if the film is thick enough, the strain effect is more dominant, and it may undergo the phase transformation into the predicted phase diagram. Experimentally a few layers of the pseudomorphic α-Ga_2O_3 on Al_2O_3 substrate[42] is a good example case. A high lattice coherence at the interface structure between α-Ga_2O_3 and Al_2O_3 can be a reason for the growth of α-Ga_2O_3. However, after growing a few layers, α-Ga_2O_3 cannot withstand the large strain effect and undergoes phase transformation into β-Ga_2O_3, which has a less strain effect. The critical thickness of the pseudomorphic growth is highly correlated with the growth temperature:[43,44] therefore, careful growth is needed for a successful phase and interface control.

We found out that the epitaxial enthalpy of mixing is reduced by decreasing the strain effect caused by the substrate. This means that a high-quality thin film can be achieved by appropriately selecting a substrate with a small lattice mismatch with the desired phase. Also, for the phase control strategy by selecting the substrate, we selected a commercial substrate, namely $LiTaO_3$, to minimize the lattice mismatch with ε-phases. On the $LiTaO_3$ substrate, the ε-phase is the most favorable structure at a low In concentration, as shown in Figure 4c. The Gibbs energy of mixing represented in Supporting Information Figure S3b. In the phase diagram, shown in Figure 4d, the stable regions for the ε-/c-phases look like lines; on the other hand, the stable region for the h-phase becomes wider above 700 °C. We also identified a very wide metastable and a narrow unstable phase region. The circle point in the phase diagram is the experimental report for the ε-

https://doi.org/10.1021/acsaelm.2c00240
ACS Appl. Electron. Mater. 2022, 4, 2711−2717

phase grown on the $LiTaO_3(001)$ substrate.[45] According to the results of Table 1 and Figure 4, the thermodynamic stability is highly correlated with the strain effect induced by the lattice mismatch between the thin film and substrate.

CONCLUSIONS

We investigated the alloying properties of $(In_xGa_{1-x})_2O_3$ alloy structures by calculating the phase diagrams in bulk and epitaxial states. We found out that the epitaxial strain effect is crucial for the phase diagram calculation, and the strain-free phase diagram of the $(In_xGa_{1-x})_2O_3$ alloy has inconsistency with some experimental reports. This is because the strain effect from the heteroepitaxy is a dominant factor for thermodynamic stability, and its effects are largely dependent on the crystal structure of the alloy. We also identified the phase diagram of the epitaxial growth on the α-$Al_2O_3(001)$ substrate, suggesting the phase control strategy by exploiting the epitaxial strain. Furthermore, we suggest the substrate, namely $LiTaO_3$, for a high-quality thin-film growth of the ε-phase. Identifying the epitaxial phase diagrams to control the $(In_xGa_{1-x})_2O_3$ phases will pave the way to achieve a successful growth of $(In_xGa_{1-x})_2O_3$ thin films for the fabrication of high-power electronics and optoelectronics devices.

ASSOCIATED CONTENT

Supporting Information

The Supporting Information is available free of charge at https://pubs.acs.org/doi/10.1021/acsaelm.2c00240.

SQS model for alloy polymorphs, lattice constants of Ga_2O_3 polymorphs and each substrate, difference for the enthalpies of mixing by different alloy models, CSL model of alloy, and epitaxial Gibbs free energy of mixing for β- and ε-phases (PDF)

AUTHOR INFORMATION

Corresponding Author

Sung Beom Cho − *Center of Materials Digitalization, Korea Institute of Ceramic Engineering and Technology (KICET), Jinju 52851, Republic of Korea;* orcid.org/0000-0002-3151-0113; Email: csb@kicet.re.kr

Authors

Han Uk Lee − *Center of Materials Digitalization, Korea Institute of Ceramic Engineering and Technology (KICET), Jinju 52851, Republic of Korea; Department of Materials Engineering, Gyeongsang National University, Jinju 52828, Republic of Korea;* orcid.org/0000-0003-1631-260X

Hyeon Woo Kim − *Center of Materials Digitalization, Korea Institute of Ceramic Engineering and Technology (KICET), Jinju 52851, Republic of Korea; Department of Materials Science and Engineering, Hanyang University, Seoul 04763, Republic of Korea*

Giulio Fatti − *Center of Materials Digitalization, Korea Institute of Ceramic Engineering and Technology (KICET), Jinju 52851, Republic of Korea;* orcid.org/0000-0001-7000-7310

Hyunseok Ko − *Center of Materials Digitalization, Korea Institute of Ceramic Engineering and Technology (KICET), Jinju 52851, Republic of Korea;* orcid.org/0000-0002-1891-6194

Complete contact information is available at: https://pubs.acs.org/10.1021/acsaelm.2c00240

Author Contributions

‖H.U.L. and H.W.K. contributed equally.

Notes

The authors declare no competing financial interest.

ACKNOWLEDGMENTS

The authors gratefully acknowledge the support from the National Research Foundation of Korea (NRF-2020M3H4A3081796). The computations were carried out using resources from the Korea Supercomputing Center (KSC-2021-RND-0025).

REFERENCES

(1) Galazka, Z. β-Ga_2O_3 for wide-bandgap electronics and optoelectronics. *Semicond. Sci. Technol.* **2018**, *33*, 113001.

(2) Pearton, S. J.; Ren, F.; Tadjer, M.; Kim, J. Perspective: Ga_2O_3 for ultra-high power rectifiers and MOSFETS. *J. Appl. Phys.* **2018**, *124*, 220901.

(3) Ranga, P.; Cho, S. B.; Mishra, R.; Krishnamoorthy, S. Highly tunable, polarization-engineered two-dimensional electron gas in ε-$AlGaO_3$/ε-Ga_2O_3 heterostructures. *Appl. Phys. Express* **2020**, *13*, 061009.

(4) Wang, T.; Li, W.; Ni, C.; Janotti, A. Band Gap and Band Offset of Ga_2O_3 and $(Al_xGa_{1-x})_2O_3$ Alloys. *Phys. Rev. Appl.* **2018**, *10*, 011003.

(5) Anhar Uddin Bhuiyan, A. F. M.; Feng, Z.; Johnson, J. M.; Chen, Z.; Huang, H.-L.; Hwang, J.; Zhao, H. MOCVD epitaxy of β-$(Al_xGa_{1-x})_2O_3$ thin films on (010) Ga_2O_3 substrates and N-type doping. *Appl. Phys. Lett.* **2019**, *115*, 120602.

(6) Nishinaka, H.; Miyauchi, N.; Tahara, D.; Morimoto, S.; Yoshimoto, M. Incorporation of indium into ε-gallium oxide epitaxial thin films grown via mist chemical vapour deposition for bandgap engineering. *CrystEngComm* **2018**, *20*, 1882−1888.

(7) Suzuki, N.; Kaneko, K.; Fujita, S. Growth of corundum-structured $(In_xGa_{1-x})_2O_3$ alloy thin films on sapphire substrates with buffer layers. *J. Cryst. Growth* **2014**, *401*, 670−672.

(8) Gottschalch, V.; Merker, S.; Blaurock, S.; Kneiß, M.; Teschner, U.; Grundmann, M.; Krautscheid, H. Heteroepitaxial growth of α-, β-, γ- and κ-Ga_2O_3 phases by metalorganic vapor phase epitaxy. *J. Cryst. Growth* **2019**, *510*, 76−84.

(9) Roy, R.; Hill, V. G.; Osborn, E. F. Polymorphism of Ga_2O_3 and the System Ga_2O_3—H_2O. *J. Am. Chem. Soc.* **1952**, *74*, 719−722.

(10) Kaun, S. W.; Wu, F.; Speck, J. S. β-$(Al_xGa_{1-x})_2O_3$/Ga_2O_3 (010) heterostructures grown on β-Ga_2O_3 (010) substrates by plasma-assisted molecular beam epitaxy. *J. Vac. Sci. Technol., A* **2015**, *33*, 041508.

(11) Oshima, T.; Okuno, T.; Arai, N.; Kobayashi, Y.; Fujita, S. β-$Al_{2x}Ga_{2-2x}O_3$ Thin Film Growth by Molecular Beam Epitaxy. *Jpn. J. Appl. Phys.* **2009**, *48*, 070202.

(12) Ito, H.; Kaneko, K.; Fujita, S. Growth and Band Gap Control of Corundum-Structured \alpha-$(AlGa)_2O_3$ Thin Films on Sapphire by Spray-Assisted Mist Chemical Vapor Deposition. *Jpn. J. Appl. Phys.* **2012**, *51*, 100207.

(13) Peelaers, H.; Steiauf, D.; Varley, J. B.; Janotti, A.; Van de Walle, C. G. $(In_xGa_{1-x})_2O_3$ alloys for transparent electronics. *Phys. Rev. B: Condens. Matter Mater. Phys.* **2015**, *92*, 085206.

(14) Zhang, F.; Saito, K.; Tanaka, T.; Nishio, M.; Guo, Q. Wide bandgap engineering of $(GaIn)_2O_3$ films. *Solid State Commun.* **2014**, *186*, 28−31.

(15) Kokubun, Y.; Abe, T.; Nakagomi, S. Sol−gel prepared $(Ga_{1-x}In_x)_2O_3$ thin films for solar-blind ultraviolet photodetectors. *Phys. Status Solidi A* **2010**, *207*, 1741−1745.

(16) Kim, H. W.; Ko, H.; Chung, Y.-C.; Cho, S. B. Heterostructural phase diagram of Ga2O3−based solid solution with Al2O3. *J. Eur. Ceram. Soc.* **2021**, *41*, 611−616.

(17) Peelaers, H.; Varley, J. B.; Speck, J. S.; Van de Walle, C. G. Structural and electronic properties of Ga_2O_3-Al_2O_3 alloys. *Appl. Phys. Lett.* **2018**, *112*, 242101.

(18) Maccioni, M. B.; Fiorentini, V. Phase diagram and polarization of stable phases of $(Ga_{1-x}In_x)_2O_3$. *Appl. Phys. Express* **2016**, *9*, 041102.
(19) Shannon, R. D.; Prewitt, C. T. Synthesis and structure of phases in the In_2O_3-Ga_2O_3 system. *J. Inorg. Nucl. Chem.* **1968**, *30*, 1389−1398.
(20) Oshima, T.; Fujita, S. Properties of Ga_2O_3-based $(In_xGa_{1-x})_2O_3$ alloy thin films grown by molecular beam epitaxy. *Phys. Status Solidi C* **2008**, *5*, 3113−3115.
(21) Kneiß, M.; Hassa, A.; Splith, D.; Sturm, C.; von Wenckstern, H.; Lorenz, M.; Grundmann, M. Epitaxial stabilization of single phase κ-$(In_xGa_{1-x})_2O_3$ thin films up to x = 0.28 on c-sapphire and κ-Ga_2O_3(001) templates by tin-assisted VCCS-PLD. *APL Mater.* **2019**, *7*, 101102.
(22) Fares, C.; Kneiß, M.; von Wenckstern, H.; Grundmann, M.; Tadjer, M.; Ren, F.; Lambers, E.; Pearton, S. J. Valence band offsets for ALD SiO_2 and Al_2O_3 on $(In_xGa_{1-x})_2O_3$ for x = 0.25−0.74. *APL Mater.* **2019**, *7*, 071115.
(23) von Wenckstern, H. Properties of (In,Ga)2O3 alloys. In *Gallium Oxide*; Pearton, S., Ren, F., Mastro, M., Eds.; Elsevier, 2019; Chapter 6, pp 119−148.
(24) Wouters, C.; Sutton, C.; Ghiringhelli, L. M.; Markurt, T.; Schewski, R.; Hassa, A.; von Wenckstern, H.; Grundmann, M.; Scheffler, M.; Albrecht, M. Investigating the ranges of (meta)stable phase formation in $(In_xGa_{1-x})_2O_3$: Impact of the cation coordination. *Phys. Rev. Mater.* **2020**, *4*, 12.
(25) von Wenckstern, H.; Splith, D.; Werner, A.; Müller, S.; Lorenz, M.; Grundmann, M. Properties of Schottky Barrier Diodes on $(In_xGa_{1-x})_2O_3$ for $0.01 \leq x \leq 0.85$ Determined by a Combinatorial Approach. *ACS Comb. Sci.* **2015**, *17*, 710−715.
(26) Baldini, M.; Gogova, D.; Irmscher, K.; Schmidbauer, M.; Wagner, G.; Fornari, R. Heteroepitaxy of Ga2 (1-x) In2xO3 layers by MOVPE with two different oxygen sources. *Cryst. Res. Technol.* **2014**, *49*, 552−557.
(27) Kresse, G.; Furthmüller, J. Efficient iterative schemes for ab initio total-energy calculations using a plane-wave basis set. *Phys. Rev. B: Condens. Matter Mater. Phys.* **1996**, *54*, 11169−11186.
(28) Blöchl, P. E. Projector augmented-wave method. *Phys. Rev. B* **1994**, *50*, 17953−17979.
(29) Perdew, J. P.; Burke, K.; Ernzerhof, M. Generalized Gradient Approximation Made Simple. *Phys. Rev. Lett.* **1996**, *77*, 3865−3868.
(30) Zunger, A.; Wei, S.-H.; Ferreira, L. G.; Bernard, J. E. Special quasirandom structures. *Phys. Rev. Lett.* **1990**, *65*, 353−356.
(31) van de Walle, A.; Tiwary, P.; de Jong, M.; Olmsted, D. L.; Asta, M.; Dick, A.; Shin, D.; Wang, Y.; Chen, L.-Q.; Liu, Z.-K. Efficient stochastic generation of special quasirandom structures. *Calphad* **2013**, *42*, 13−18.
(32) Bollmann, W. *Crystal Defects and Crystalline Interfaces*; Springer Berlin Heidelberg, 1970.
(33) Pasquevich, A. F.; Uhrmacher, M.; Ziegeler, L.; Lieb, K. P. Hyperfine interactions of ^{111}Cd in Ga_2O_3. *Phys. Rev. B: Condens. Matter Mater. Phys.* **1993**, *48*, 10052−10062.
(34) Edwards, D. D.; Folkins, P. E.; Mason, T. O. Phase Equilibria in the $Ga_2O_3In_2O_3$ System. *J. Am. Ceram. Soc.* **1997**, *80*, 253−257.
(35) Farvid, S. S.; Wang, T.; Radovanovic, P. V. Colloidal gallium indium oxide nanocrystals: a multifunctional light-emitting phosphor broadly tunable by alloy composition. *J. Am. Chem. Soc.* **2011**, *133*, 6711−6719.
(36) Hassa, A.; von Wenckstern, H.; Splith, D.; Sturm, C.; Kneiß, M.; Prozheeva, V.; Grundmann, M. Structural, optical, and electrical properties of orthorhombic κ-$(In_xGa_{1-x})_2O_3$ thin films. *APL Mater.* **2019**, *7*, 022525.
(37) Yang, F.; Ma, J.; Luan, C.; Kong, L. Structural and optical properties of $Ga_{2(1-x)}In_{2x}O_3$ films prepared on α-Al_2O_3 (0001) by MOCVD. *Appl. Surf. Sci.* **2009**, *255*, 4401−4404.
(38) Zhang, F.; Li, H.; Arita, M.; Guo, Q. Ultraviolet detectors based on (GaIn) 2 O 3 films. *Opt. Mater. Express* **2017**, *7*, 3769−3779.
(39) Cho, S. B.; Mishra, R. Epitaxial engineering of polar ε-Ga2O3 for tunable two-dimensional electron gas at the heterointerface. *Appl. Phys. Lett.* **2018**, *112*, 162101.
(40) Liu, X.; Tan, C.-K. Electronic properties of monoclinic $(In_xGa_{1-x})_2O_3$ alloys by first-principle. *AIP Adv.* **2019**, *9*, 035318.
(41) Kranert, C.; Lenzner, J.; Jenderka, M.; Lorenz, M.; von Wenckstern, H.; Schmidt-Grund, R.; Grundmann, M. Lattice parameters and Raman-active phonon modes of $(In_xGa_{1-x})_2O_3$ for x < 0.4. *J. Appl. Phys.* **2014**, *116*, 013505.
(42) Schewski, R.; Wagner, G.; Baldini, M.; Gogova, D.; Galazka, Z.; Schulz, T.; Remmele, T.; Markurt, T.; Von Wenckstern, H.; Grundmann, M.; Bierwagen, O.; Vogt, P.; Albrecht, M. Epitaxial stabilization of pseudomorphic α-Ga2O3 on sapphire (0001). *Appl. Phys. Express* **2014**, *8*, 011101.
(43) Sohi, P.; Martin, D.; Grandjean, N. Critical thickness of GaN on AlN: impact of growth temperature and dislocation density. *Semicond. Sci. Technol.* **2017**, *32*, 075010.
(44) Takane, H.; Kaneko, K.; Ota, Y.; Fujita, S. Initial nucleation scheme of Ga_2O_3 on (0001) sapphire by mist CVD for the growth of α-phase. *Jpn. J. Appl. Phys.* **2021**, *60*, 055501.
(45) Shimazoe, K.; Nishinaka, H.; Arata, Y.; Tahara, D.; Yoshimoto, M. Phase control of α-and κ-Ga2O3 epitaxial growth on LiNbO3 and LiTaO3 substrates using α-Fe2O3 buffer layers. *AIP Adv.* **2020**, *10*, 055310.

https://doi.org/10.1021/acsaelm.2c00240
ACS Appl. Electron. Mater. 2022, 4, 2711−2717